ORIGINAL PAPER

Computational analysis of the effect of the type of LVAD flow on coronary perfusion and ventricular afterload

**Ki Moo Lim · In Su Kim · Seong Wook Choi ·
Byung Goo Min · Yong Soon Won ·
Heon Young Kim · Eun Bo Shim**

Abstract We developed a computational model to investigate the hemodynamic effects of a pulsatile left ventricular assist device (LVAD) on the cardiovascular system. The model consisted of 16 compartments for the cardiovascular system, including coronary circulation and LVAD, and autonomic nervous system control. A failed heart was modeled by decreasing the end-systolic elastance of the ventricle and blocking the mechanism controlling heart contractility. We assessed the physiological effect of the LVAD on the cardiovascular system for three types of LVAD flow: co-pulsation, counter-pulsation, and continuous flow modes. The results indicated that the pulsatile LVAD with counter-pulsation mode gave the most physiological coronary blood perfusion. In addition, the counter-pulsation mode resulted in a lower peak pressure of the left ventricle than the other modes, aiding cardiac recovery by reducing the ventricular afterload. In conclusion, these results indicate that, from the perspective of cardiovascular physiology, a pulsatile LVAD with counter-pulsation operation is a plausible alternative to the existing LVAD with continuous flow mode.

Introduction

A left ventricular assist device (LVAD) is an electro-mechanical device that is used to partially replace the function of a failing heart, helping to circulate blood to the body. The main purpose of an LVAD is as a bridge to recovery, maintaining the normal cardiac output for patients in heart failure [1, 2] while benefiting the cardiac recovery effect [3–6].

These devices can be classified as pulsatile or continuous LVADs according to the pumping style. A pulsatile LVAD develops a pulsed flow, like the native pumping of the heart, whereas a continuous LVAD generates a non-pulsatile flow with no transient variation in pressure or velocity. Furthermore, pulsatile LVADs can operate in two different modes: co-pulsation and counter-pulsation modes. In the co-pulsation mode, the LVAD pumps blood in phase with the native left ventricle (LV), whereas it is out of phase in counter-pulsation mode.

The recovery of a failing ventricle is closely related to the increase in coronary blood perfusion and reduction in the ventricular afterload [7]. Evidence indicates that the counter-pulsation mechanism of an intra-aortic balloon pump increases coronary perfusion and reduces ventricular afterload [8–13]. In an animal experiment, Reesink et al. [14] showed that counter-pulsation of an extra-corporeal life support (ECLS) system decreased the LV afterload and increased coronary perfusion, aiding heart muscle recovery. However, no clear evidence demonstrates these benefits when using a pulsatile LVAD. Mathematical models of

K. M. Lim · I. S. Kim · S. W. Choi · B. G. Min ·
H. Y. Kim · E. B. Shim (✉)
Department of Mechanical and Biomedical Engineering,
Kangwon National University, Hyoja-dong, Chuncheon,
Gangwon-do, Republic of Korea
e-mail: ebshim@kangwon.ac.kr

Y. S. Won
Department of Thoracic and Cardiovascular Surgery,
College of Medicine, Soonchunhyang University,
Bucheon, Gyeonggi-do, Republic of Korea

LVAD dynamics and their effect on the cardiovascular system may help to elucidate the possible hemodynamic effects of a pulsatile LVAD at the system level. For this purpose, we developed an improved numerical model that integrated the 12-compartment model of the cardiovascular system of Heldt et al. [15], the 3-compartment model of the coronary circulation of Schreiner et al. [16], and a 1-compartment model for the LVAD. We also included an autonomic nervous system model for controlling the cardiovascular system to obtain a more realistic hemodynamic response.

Using this model, we evaluated three operating modes—co-pulsation, counter-pulsation, and continuous LVAD flow—to determine which was most advantageous for heart muscle recovery to better treat patients in heart failure using an LVAD.

Materials and methods

Model description

Sixteen-compartment cardiovascular model

The cardiovascular system model proposed by Heldt et al. [15] was modified to include the left coronary circulation model of Schreiner et al. [16] and a new LVAD model based on an experimental study [17]. Because left coronary flow constitutes 85% of total coronary flow [18], we omitted right coronary flow for simplification, as in other studies on coronary circulation [16, 19]. The model is formulated in terms of an electric analog model consisting of elements such as resistors, capacitors, and diodes. Using the hemodynamic parameters related to blood circulation, this model calculates the pressure, volume, and blood flow for each of the 16 components making up the cardiovascular system (Fig. 1): the left ventricle (lv), aorta (a), right ventricle (rv), pulmonary artery (pa), and pulmonary vein (pv); the components of the tissue circulation system including three parts of the vena cava [the superior vena cava (svc) and the inferior vena cava (ivc) inside the thoracic cavity, and the abdominal vena cava (avc) inside the abdominal cavity]; four systemic arterial branches [the upper body (up), kidneys (kid), splanchnic organs (sp), and lower limb (ll)]; coronary circulation [left circumflex artery (lcx), left anterior descending artery (lad), and coronary venous bed (cv)]; and the LVAD component (lvad). The coronary circulation component [16] is combined with the main system model in a parallel connection from the aorta to the inlet of the right heart. We also combined the LVAD compartment with the main system model in a parallel connection to the native left heart, with its inlet cannulated to the LV apex and the outlet attached to the aorta. The governing equation of the model is shown in the "Appendix."

The ventricle in the cardiovascular system can be approximated as a chamber with an entrance and an exit valve, whose compliance changes as a function of time [15]. The compliance can be replaced by a capacitor in an electric analog. With this method, the left ventricular capacitance varies between a minimum value during systole and a maximum value during diastole using predetermined functions that are taken from elastance curves obtained in animal experiments [15].

A heart-failure model was implemented by decreasing the end-systolic elastance value to 40% of normal. This produced hemodynamic results that were consistent with data reported for systolic heart-failure patients in several clinical studies [20, 21] (Fig. 2). The LVAD compartment was activated by a flow generator (Q_{lvad} in Fig. 1) with a specified mean flow rate of 5,000 ml/min for all flow types.

We synchronized the pulsatile LVAD with the native left heart in-phase to simulate co-pulsation mode, whereas the peak flows of the pulsatile LVAD and native heart alternate in counter-pulsation mode. Figure 3 shows the inlet and outlet flow rates of the LVAD and the native LV in (1) co-pulsation and (2) counter-pulsation pumping modes. The flow waveform of the LVAD was taken from data measured for a pulsatile pneumatic ventricular assist device, the Hybrid Ventricular Assist Device (H-VAD; Korea Artificial Organ Center, Seoul, Korea) [17]. The parameters of the systemic circulation and LVAD are summarized in Table 1 [15, 16].

Autonomic nervous system model

The hemodynamic properties of the cardiovascular system are modulated by a network of homeostasis-maintaining feedback mechanisms. This feedback control system must account for the major reflex mechanisms that govern the short-term behavior of the cardiovascular system, i.e., the two major neurally mediated cardiovascular reflexes: the arterial baroreflex and cardiopulmonary reflex. A schematic representation of the regulatory system is depicted in Fig. 4. This figure shows the autonomous nerve control with the baroreceptor reflex and cardiopulmonary control systems. Locally sensed blood pressures at the carotid artery (P_A) and central vein (P_{CV}) are relayed to the autonomic nervous system (ANS), where error signals (P_A^{eff}, P_{CV}^{eff}) are generated by subtracting pre-defined set-point values (P_A^{ref}, P_{CV}^{ref}) from the afferent pressure signals (P_A, P_{CV}). These error signals subsequently dictate the efferent activity of the reflex model, via parasympathetic and sympathetic arcs, such that the error signals in the following computational steps approach zero.

Among the four effector mechanisms implemented in the model, we blocked the control path of cardiac contractility to mimic heart failure with systolic dysfunction

Fig. 1 Circuit diagram used to model the hemodynamics of the cardiovascular system (adapted from Heldt et al. [15] and Schreiner et al. [16]). *P* Pressure, *R* flow resistance, *C* vascular compliance, *Q* flow generator, *lv* left ventricle, *a* artery, *up* upper body, *kid* kidney, *sp* splanchnic, *ll* lower limbs, *avc* abdominal vena cava, *ivc* inferior vena cava, *svc* superior vena cava, *rv* right ventricle, *pa* pulmonary artery, *pv* pulmonary vein, *th* thoracic, *is* interstitial, *sqz* squeezed from LV, *lca* left coronary artery, *lcx* left circumflex, *lad* left anterior descending artery, *cv* coronary vein, *vi* VAD inlet, *vo* VAD outlet
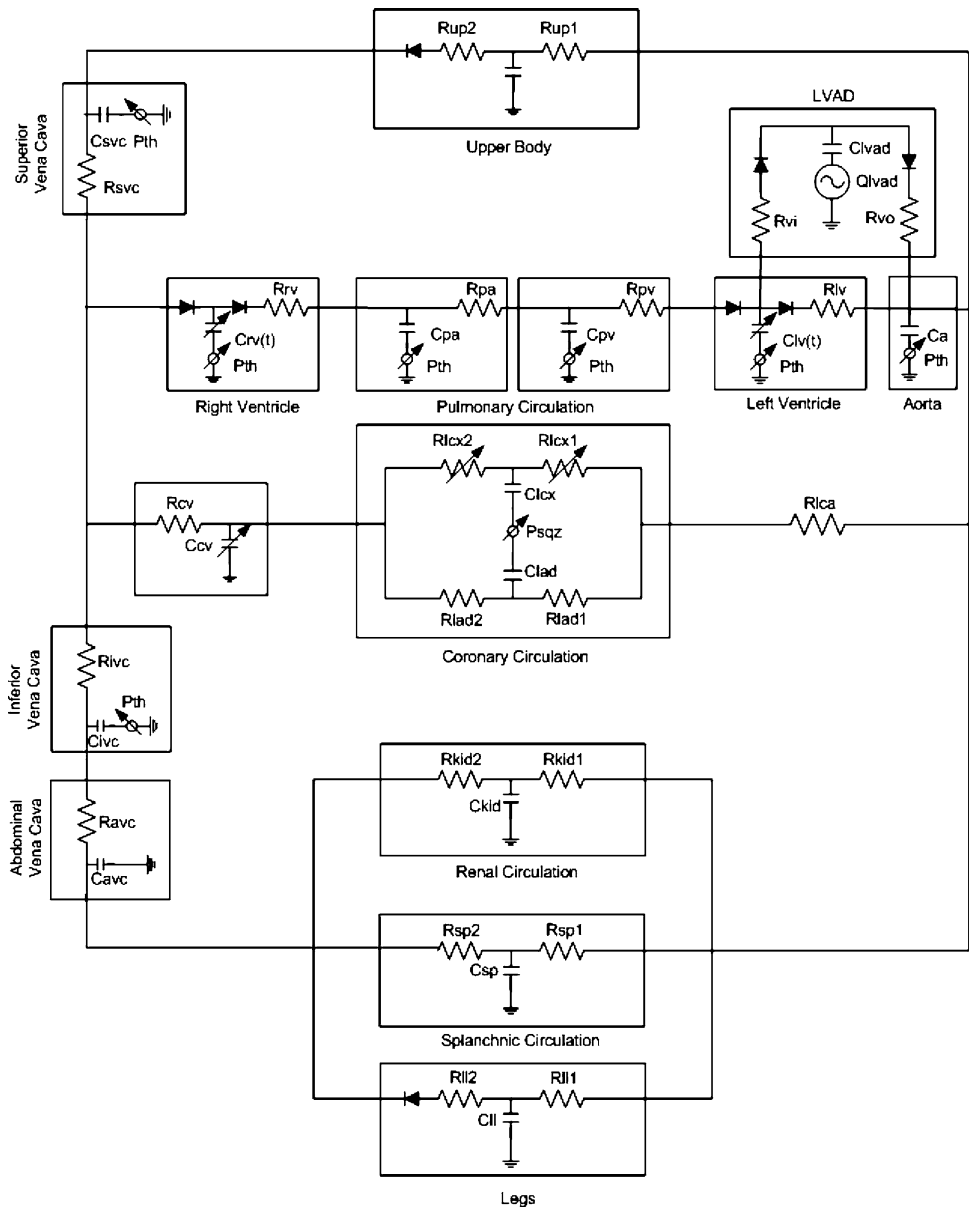
[22]. The governing equations of the system are shown in the "Appendix."

Computational setup

Applying Kirchhoff's law to each node produces 16 coupled first-order non-homogeneous differential equations as shown in the "Appendix." An adaptive step-size fourth-order Runge-Kutta method is used to integrate the differential equations numerically. The integration step size ranges from 6.1×10^{-4} s during ventricular ejection phase to a user-defined upper limit of 0.01 s during ventricular diastole, with a mean step size of 5.6×10^{-3} s. The initial pressures were estimated by a linear algebraic solution of a steady-state version of the hemodynamic system.

Results

Validation of the cardiovascular system model

To validate the cardiovascular system model, we calculated the blood pressure and flow rate at each compartment and compared them with clinical data for a normal person [18] as listed in Table 2. The simulated pressure waves at the left ventricle and systemic artery for the normal and congestive heart-failure models are shown in Fig. 5a and b, respectively. In the normal model, the mean arterial and pulse pressures were approximately 100 and 31 mmHg, respectively, and the resulting cardiac output was 5,478 ml/min. In the congestive heart-failure model, the mean arterial pressure was about 71 mmHg (71% of the
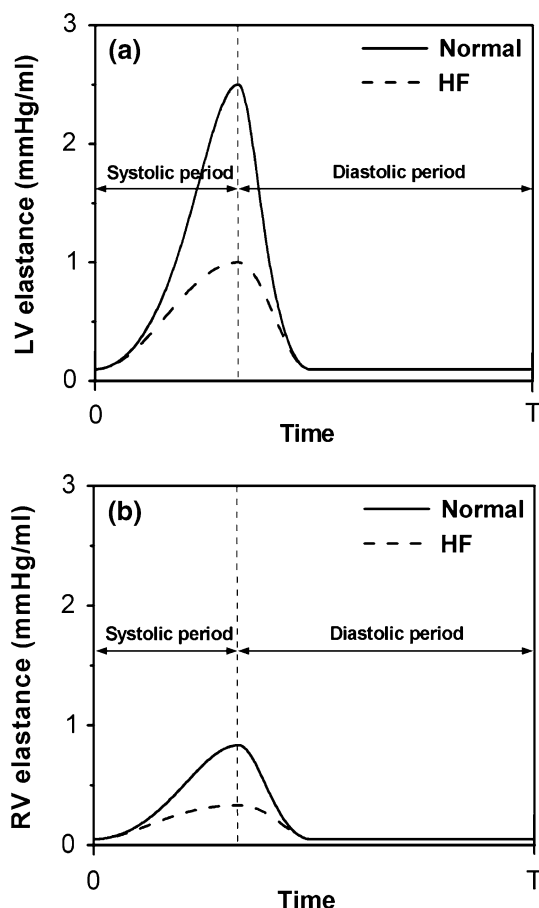
Fig. 2 Temporal changes in the elastance of the left (a) and right (b) ventricles in the normal (*straight line*) and heart-failure (*dashed line*) models. *T* Period of one cycle

normal model), the arterial pulse pressure was about 21 mmHg (68% of the normal model), and the cardiac output was 3,826 ml/min (70% of the normal model). Due to the impaired hemodynamic function in the heart-failure model, sympathetic nervous regulation was strongly activated, resulting in an increased heart rate, peripheral resistance, and venous tone compared with the normal model. More detailed data are shown in Table 3.

Cardiovascular response according to the LVAD flow type

Three different modes of LVAD pumping were simulated: a co-pulsation mode, in which the native LV and pulsatile LVAD contract simultaneously; a counter-pulsation mode, in which the pulsatile LVAD contracts out of phase with the native LV; and a continuous flow mode, in which the LVAD pumps blood continuously at a continuous flow rate.

Figure 6 illustrates the cardiovascular system responses with the LVAD implanted in the heart-failure case for the three different pumping modes: co-pulsation, counter-pulsation, and continuous flow. LVAD flow rate was set to
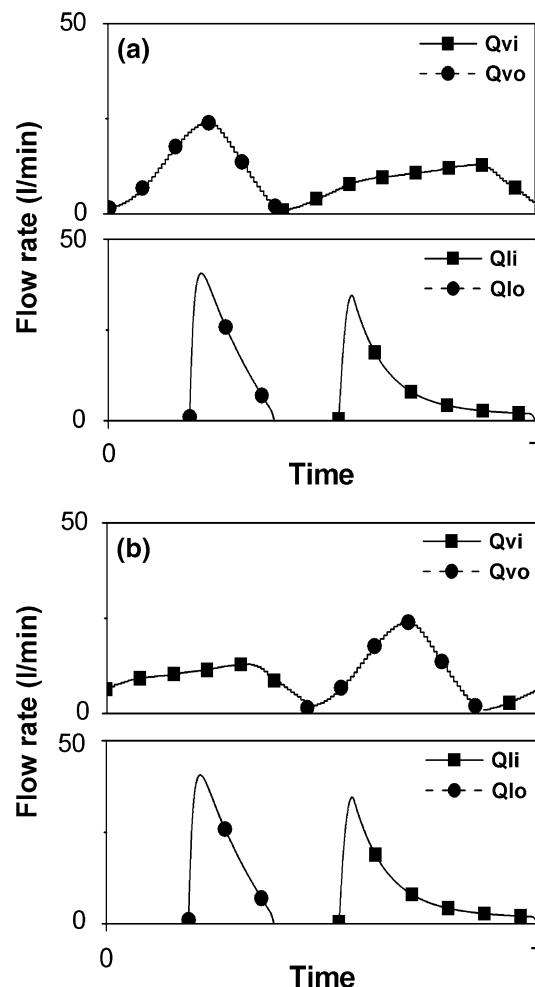

Fig. 3 Flow waveforms generated from an LVAD that produces co-pulsating (a) and counter-pulsating (b) flow compared with the native left ventricular flow waveforms. *Qvi* VAD inlet flow, *Qvo* VAD outlet flow, *Qli* left ventricular inlet flow, *Qlo* left ventricular outlet flow, *T* period of one cycle

5,000 ml/min in this simulation, and the arterial pressure greatly exceeded the LV peak pressure, as shown in Fig. 6. Therefore, the aortic valve was not open during the whole cardiac cycle and the native cardiac output was zero in this study. All the LVAD pumping modes resulted in lower LV pressures than in the model of heart failure without the LVAD. Of the three pumping modes, the co-pulsation mode generated the highest LV peak pressure (62 mmHg, Fig. 6a), followed by the continuous pumping mode (52 mmHg, Fig. 6e) and the counter-pulsation mode (44 mmHg, Fig. 6c). Therefore, the counter-pulsation mode had the lowest LV afterload and greatest benefit for heart recovery.

The temporal variation in the coronary blood-flow rate for co-pulsation, counter-pulsation, and continuous LVAD pumping modes is shown in Fig. 6b, d, f, respectively. The resistance to the coronary flow is directly related to LV pressure, and aortic pressure provides a driving force for

Table 1 Numerical values of fixed parameters [vascular resistance, zero-pressure filling volume (ZPFV), vascular compliance] used in the cardiovascular hemodynamic model (adopted from Heldt et al. [15] and Schreiner et al. [16])

	Resistance (PRU)	ZPFV (ml)	Compliance (ml/mmHg)	Reference
Right ventricle	0.003	50	1.2–20	[15]
Pulmonary arteries	0.08	90	4.3	[15]
Pulmonary veins	0.01	490	8.4	[15]
Left ventricle	0.006	50	0.4–10	[15]
Systemic arteries		715	2.0	[15]
Upper body 1	3.9	650	8	[15]
Upper body 2	0.23			[15]
Kidney 1	4.1	150	15	[15]
Kidney 2	0.3			[15]
Splanchnic 1	3.0	1,300	55	[15]
Splanchnic 2	0.18			[15]
Lower limb 1	3.6	350	19	[15]
Lower limb 2	0.3			[15]
AVC	0.01	250	25	[15]
IVC	0.015	75	2	[15]
SVC	0.06	10	15	[15]
LCX 1	27	0	0.2	[16]
LCX 2	2.7			[16]
LAD 1	27	0	0.2	[16]
LAD 2	2.7			[16]
CV	0.6	25		[16]
LCA	0.05			[16]

AVC Abdominal vena cava, *IVC* inferior vena cava, *SVC* superior vena cava, *LCX* left circumflex artery, *LAD* left anterior descending artery, *LCA* left coronary artery, *CV* coronary vein

Fig. 4 Diagrammatic representation of the baroreflex model. *A* Artery, *CV* central vein, *CS* carotid sinus, *CP* cardiopulmonary, *ref* reference, *ANS* autonomic nervous system, *SA node* sinoatrial node, *Σ* summation
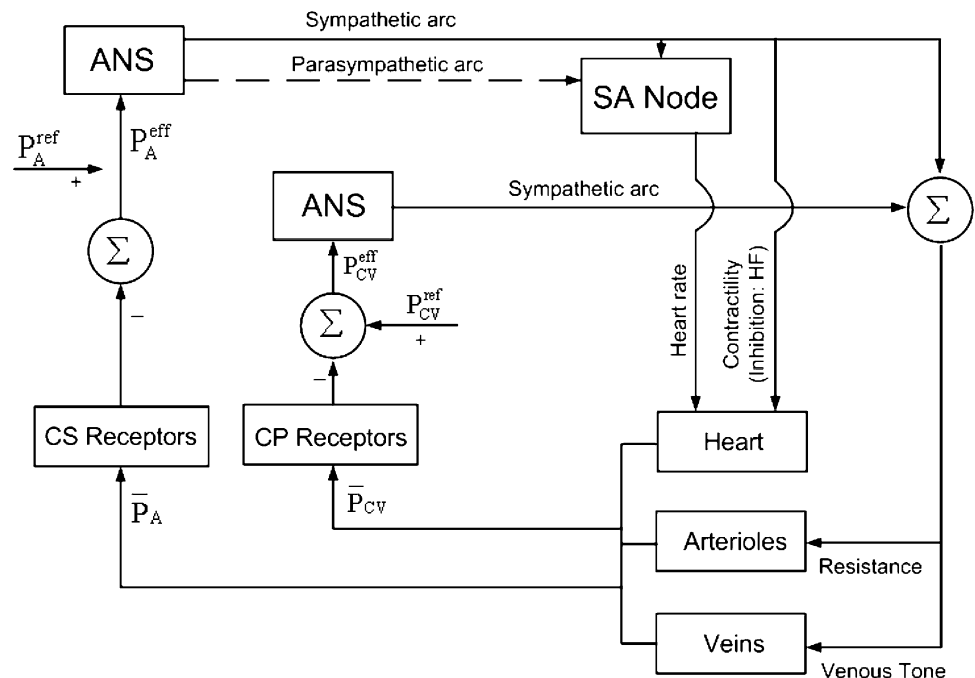
the coronary flow. As a result, during systole, the largest driving force was counterbalanced by the largest resistive force in co-pulsation mode whereas the smallest driving force was balanced by the smallest resistive force in counter-pulsation mode. This logic can also be applied to continuous flow mode. Therefore, there was not a significant difference in the coronary flow rate among the three modes during systole. During diastole, LV pressure was

Springer

Table 2 Comparison of the simulated results with a set of norms from the literature [15]

Variables	Normal range (Heldt et al. [15])	Present simulation
LV pressure (mmHg)		
Systole	90–140	117
Diastole	4–12	8
Arterial pressure (mmHg)		
Systole	90–140	117
Diastole	60–90	84
Cardiac output (ml/min)	4,700–7,100	5,478
Stroke volume (ml)	51–110	76
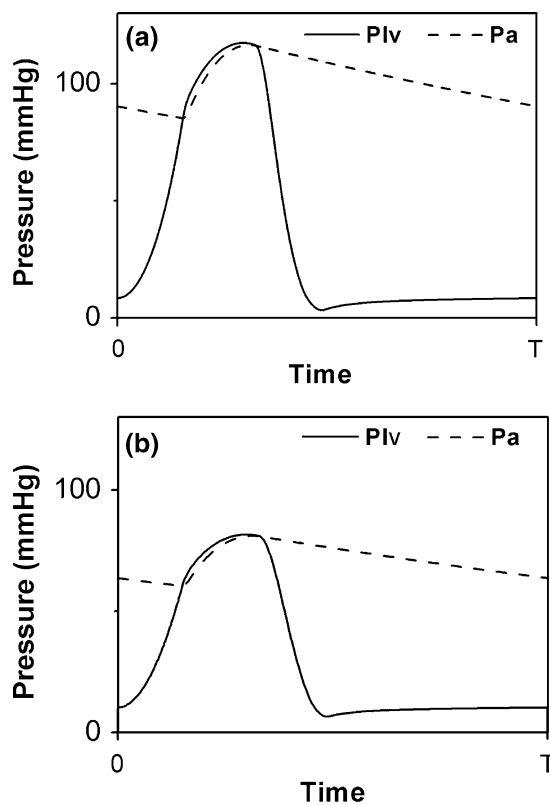
Fig. 5 Simulated pressure waveforms in the left ventricle and systemic artery for **a** a normal and **b** the congestive heart-failure model. *Plv* Left ventricular pressure, *Pa* systemic arterial pressure, *T* period of one cycle

nearly zero regardless of pumping mode, and the arterial pressure induced by LVAD was highest in counter-pulsation mode, intermediate in continuous flow mode, and lowest in co-pulsation mode. Thus, counter-pulsation mode developed the highest coronary flow (Fig. 6d), then continuous flow mode (Fig. 6f), and co-pulsation mode developed the lowest coronary flow during diastole and also during one pumping cycle (Fig. 6b).

Table 3 Simulated hemodynamic responses of a normal person, a patient with heart failure, and a patient with heart failure with an LVAD operating in co-pulsation, counter-pulsation, and continuous flow modes

	Normal	HF	LVAD-implanted HF		
			Co	Counter	Cont
LVAD flow (ml/min)	0	0	5,000	5,000	5,000
Native cardiac output (ml/min)	5,478	3,826	0	0	0
Stroke volume (ml)	76	37	0	0	0
Blood flow: lca (ml/min)	247	156	298	314	302
Blood flow: up (ml/min)	1,418	1,105	1,221	1,218	1,217
Blood flow: sp (ml/min)	1,857	1,427	1,574	1,571	1,568
Blood flow: ll (ml/min)	1,510	1,173	1,296	1,293	1,292
Blood flow: kid (ml/min)	693	552	599	597	597
MAP (mmHg)	100	71	89	89	89
Pulse aortic pressure (mmHg)	31	21	17	17	0
LV peak pressure (mmHg)	117	82	62	43	51
Heart rate (bpm)	72	103	93	93	93
Peripheral resistance: up (%)	100	105	99	98	98
Peripheral resistance: sp (%)	100	107	98	97	98
Peripheral resistance: ll (%)	100	106	98	98	98
Peripheral resistance: kid (%)	100	102	99	99	99
ZPFV: up (%)	100	98	100	100	100
ZPFV: sp (%)	100	97	100	100	100
ZPFV: ll (%)	100	97	100	100	100
ZPFV: kid (%)	100	98	100	100	100

HF Heart-failure patient, *Co* co-pulsation, *Counter* counter-pulsation, *Cont* continuous, *lca* left coronary artery, *up* upper body, *sp* splanchnic, *ll* lower limbs, *kid* kidney, *MAP* mean arterial pressure, *LV* left ventricle, *ZPFV* zero-pressure filling volume

Figure 7 shows the coronary and upper-body perfusion rates in the normal and LVAD-implanted heart-failure models as the percentage of perfusion in a heart-failure model without LVAD. In the heart-failure model, coronary perfusion was reduced to 63% of the normal perfusion. This would induce ischemic disease, worsening heart failure. When the LVAD was used in the heart-failure model, coronary perfusion was increased and even exceeded the normal perfusion. The percent increases in coronary flow relative to that for heart failure were 91, 101, and 93% for the co-pulsation, counter-pulsation, and continuous flow modes, respectively. We also considered the blood perfusion rate for other compartments, including the kidneys, splanchnic region, lower limbs, and upper body. Because cerebral circulation is a major part of the upper body circulation, we assumed that upper-body perfusion reflects cerebral perfusion directly. Although the LVAD pumping increased upper-body perfusion, no significant difference was found among the three pumping modes

Fig. 6 Simulated pressure waveforms in the left ventricle and systemic artery for the LVAD-implanted heart-failure model operating in **a** co-pulsation, **c** counter-pulsation, and **e** continuous flow mode. Simulated flow waveforms through the LV inlet and coronary artery in **b** co-pulsation, **d** counter-pulsation, and **f** continuous flow mode. P_{lv} Left ventricular pressure, P_a systemic arterial pressure, Q_{li} left ventricle inlet flow, Q_{cor} coronary artery flow, T period of one cycle
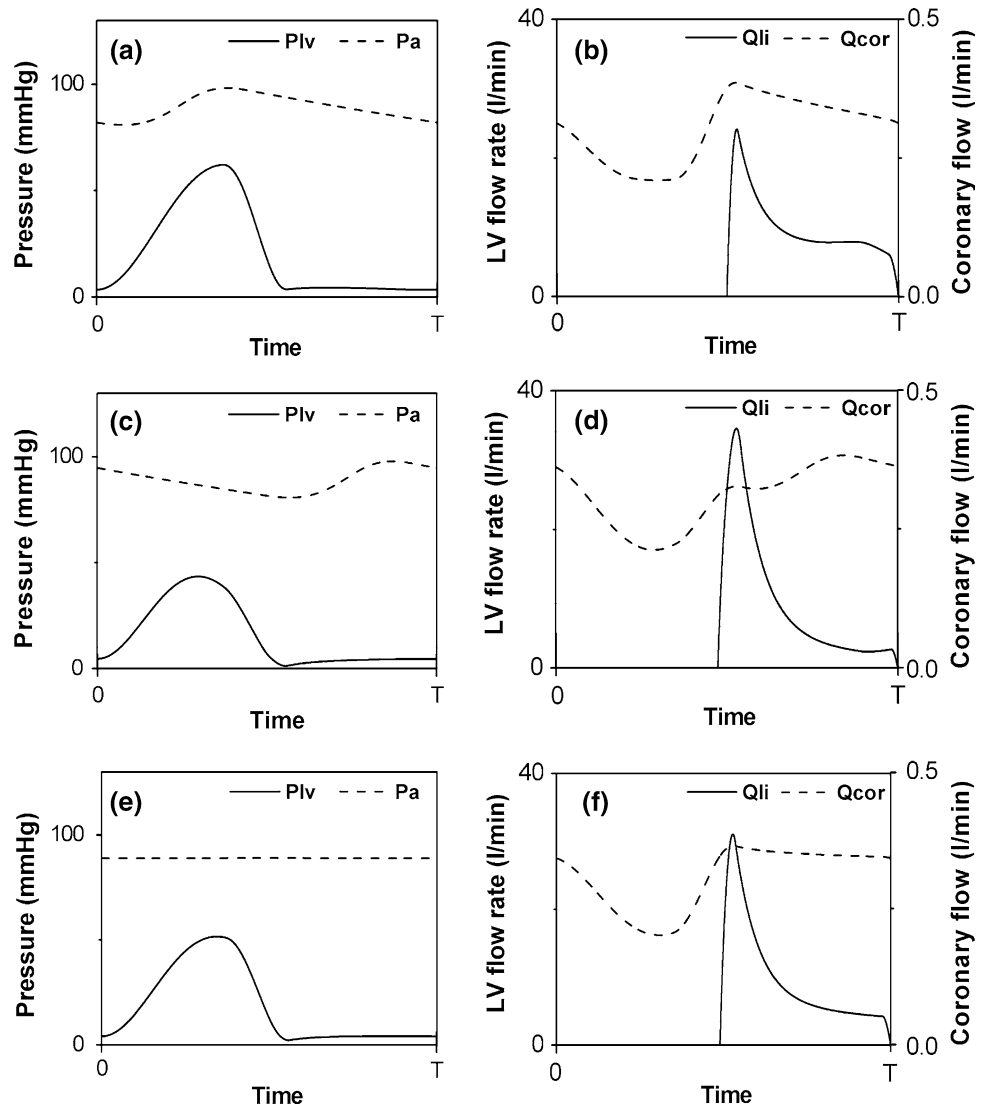
(Fig. 7). The perfusion of other tissues, such as the kidneys, splanchnic region, and lower limbs, showed the same tendency as upper-body circulation.

Discussion

This study determined the physiological effects of an LVAD on the cardiovascular response according to the pumping mode used (co-pulsation, counter-pulsation, and continuous flow modes), focusing on variations in coronary perfusion and ventricular peak pressure associated with the three modes. Improved coronary perfusion and reduced ventricular peak pressure are considered as indicators of cardiac muscle recovery [7].

The heart-failure model was implemented by decreasing the end-systolic ventricular elastance and inhibiting the sympathetic control of cardiac contractility. Therefore,
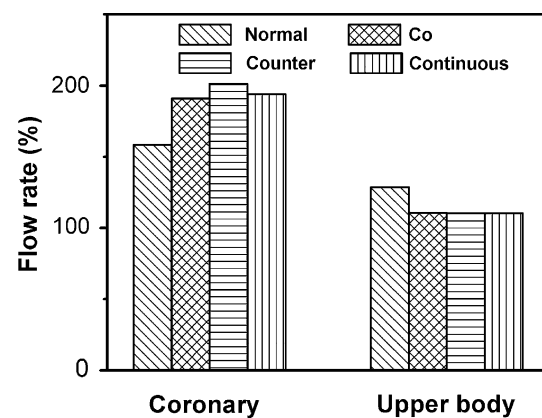

Fig. 7 Coronary and upper-body perfusion rates in the normal model (*Normal*), and an LVAD-implanted heart failure case in co-pulsation (*Co*), counter-pulsation (*Counter*), and continuous flow (*Continuous*) modes. The results are given as the percent increase in perfusion relative to that of a heart-failure model

ventricular contractile force is weakened, and there is no compensatory mechanism for recovering cardiac contractility. Consequently, the ventricular stroke volume was reduced (Table 3), which in turn decreased cardiac output, arterial pressure, and tissue perfusion. The regulatory ANS was activated to compensate for the reduced arterial and central venous pressure by increasing the heart rate, vascular resistance, and venous tone, according to Eqs. 8–10 in the "Appendix."

In the LVAD-implanted heart-failure model, the systolic arterial pressure was the highest in co-pulsation mode, due to the synchronized contraction of the native ventricle and LVAD. Consequently, a high load was imposed on the ventricular tissue, resulting in a high pressure in the LV. In the counter-pulsation mode, alternate pumping between the LV and LVAD kept the systolic arterial pressure low, reducing the pressure in the LV. During the LVAD pumping cycle, the aortic valve remains closed because the aortic pressure is higher than the ventricular pressure.

In contrast to other capillary beds, blood flow to the coronary vessels is lower during systole because of the strong compression of the left ventricular muscle around the intramuscular vessels during cardiac contraction. During diastole, the cardiac muscles relax and no longer impede blood flow through the ventricular capillaries, so that coronary blood flows more freely. To model this mechanism, we used the intra-myocardial pressure of coronary vessels, which is correlated with the ventricular pressure and a volume-dependent resistance term from Schreiner et al. [16] as shown in the "Appendix".

The computational results showed that the counter-pulsating LVAD pumping mode was more effective for coronary perfusion than the other modes. Due to the increased intra-myocardial pressure affecting the coronary vessels during systole, which increased the flow resistance, the LVAD contraction during systole in co-pulsation mode was not effective for supplying blood to the coronary capillaries. Therefore, the counter-pulsating LVAD pumping mode showed the best performance in terms of coronary perfusion compared with the other two modes.

Unlike the coronary vessels, the perfusion of the peripheral organs (upper body, splanchnic, lower limb, and kidney tissue) was similar regardless of pumping mode, because the flow resistance in the peripheral tissues is not related to the ventricular pressure directly. In addition, in the regulatory ANS, the flow resistances and vessel tones of the peripheral circulation are related only to the mean arterial pressure and central venous pressure [15].

The LV and aortic pressures varied with the LVAD pumping mode. According to the simulated results, the counter-pulsation mode resulted in a relatively low peak aortic pressure and reduced afterload compared with the other modes. This should benefit the recovery of the patient's heart.

In conclusion, we developed an improved numerical model that consists of 16 compartments to simulate the cardiovascular system, including the coronary circulation, when an LVAD is used to assist heart function in a heart-failure model. By simulating three different pumping modes of the LVAD (co-pulsation, counter-pulsation, and continuous flow), we demonstrated that high coronary perfusion and a low afterload could be obtained by using counter-pulsation mode. This indicates that the pulsatile LVAD can help with the cardiac muscle recovery of the impaired heart by using counter-pulsation mode. Therefore, from the perspective of cardiovascular physiology, a pulsatile LVAD with counter-pulsation operation is a plausible alternative to the current dominant type of LVAD with continuous flow mode.

Appendix

Governing equations of the hemodynamic model

The time derivative of the sixteen-compartmental volume can be expressed as

$$\frac{\mathrm{d}V_i(t)}{\mathrm{d}t} = Q_{i,\text{in}}(t) - Q_{i,\text{out}}(t) \tag{1}$$

where V indicates volume, Q is blood flow rate, t indicates time, i means each compartmental index, in means inflow to i node, and out means outflow from i node.

Each compartmental pressure is calculated as:

$$P_i(t) = P_{i,\text{ex}}(t) + \frac{V_i(t) - V_{i,d}}{C_i} \tag{2}$$

where $P_{i,\text{ex}}$ indicates extra-vascular pressure in the i compartment, which includes thoracic pressure in ventricular compartments, pulmonary compartments, superior and inferior vena cava compartments, and LV squeezing pressure in the left coronary compartments; and $V_{i,d}$ indicates dead volume in the i compartment. Thoracic pressure (th) and LV squeezing pressure (sqz) are shown below.

$$P_{i,\text{th}}(t) = -5 + \sin(0.4\pi t) \tag{3}$$

$$P_{i,\text{sqz}}(t) = \gamma_{\text{norm}} P_{lv}(t) \tag{4}$$

where γ_{norm} is the proportionality factor for LV squeezing.

Compliance of coronary vein is defined in terms of volume-dependent compliance as in the equation below. This explains the characteristic of increasing vessel stiffness with progressive distension.

$$C_{cv}(V_{cv}) = x[1 + \sigma V_{cv}(t)]^{-1} \cdot \exp[-\sigma(V_{cv}(t) - V_{cv,d})] \quad (5)$$

where cv indicates coronary vein, and x and σ are derived coefficients for the equation.

Flow resistance of left circumflex artery is not constant but has a volume-dependent value as in the equations below.

$$R_{LCX1}(t) = \begin{cases} R_{LCX} & \text{when } p_{bif} - p_{cap} > 0 \\ R_{LCX} + \beta/(V_{LCX}(t))^2 & \text{when } p_{bif} - p_{cap} < 0 \end{cases} \quad (6)$$

$$R_{LCX2}(t) = \begin{cases} R_{LCX} + \beta/(V_{LCX}(t))^2 & \text{when } p_{cap} - p_{ven} > 0 \\ R_{LCX} & \text{when } p_{cap} - p_{ven} < 0 \end{cases} \quad (7)$$

Governing equations of the baroreflex model

The variables input to the control system are the effective blood pressure deviations, which are P_A^{eff} for the arterial baroreflex and P_{CV}^{eff} for the cardiopulmonary reflex system, calculated as shown below.

$$P_A^{eff} = 18\tan^{-1}\left(\frac{\bar{P}_A - \bar{P}_A^{ref}}{18}\right) \quad (8)$$

$$P_{CV}^{eff} = 5\tan^{-1}\left(\frac{\bar{P}_{CV} - \bar{P}_{CV}^{ref}}{18}\right) \quad (9)$$

where $\bar{P}_A$ is the mean arterial pressure, $\bar{P}_{CV}$ is the mean central venous pressure, and $\bar{P}_A^{ref}$ and $\bar{P}_{CV}^{ref}$ are predefined set-point values.

The contribution of the reflex control system to the instantaneous control variables [R−R interval (which determines the heart rate), peripheral resistance, ZPFV (which indicates venous tone), and ventricular systolic compliance in the normal case only (which indicates cardiac contractility)] at time t was calculated as follows:

$$J(t) = J_0 + \int_{k=0}^{k=30} P_A^{eff}(t-k) \cdot [a \cdot p(k) + b \cdot s(k)]dk \quad (10)$$

where $J(t)$ indicates a control variable, J_0 is the baseline value of the control variable, $p(k)$ and $s(k)$ are the parasympathetic and sympathetic impulse response functions, respectively, and a and b are gain values for the respective reflex arcs.

References

1. Casarotto D, Bottio T, Gambino A, Testolin L, Gerosa G (2003) The last to die is hope: prolonged mechanical circulatory support with a Novacor left ventricular assist device as a bridge to transplantation. J Thorac Cardiovasc Surg 125(2):417–418. doi:10.1067/mtc.2003.131

2. Goldstein DJ (2003) Worldwide experience with the MicroMed DeBakey ventricular assist device as a bridge to transplantation. Circulation 108(Suppl 1):II272–II277. doi:10.1161/01.cir.0000087387.02218.7e

3. Cianci P, Lonergan-Thomas H, Slaughter M, Silver MA (2003) Current and potential applications of left ventricular assist devices. J Cardiovasc Nurs 18:17–22

4. Kumpati GS, McCarthy PM, Hoercher KJ (2001) Left ventricular assist device bridge to recovery: a review of the current status. Ann Thorac Surg 71(3 Suppl):S103–S108. doi:10.1016/S0003-4975(00)02630-8

5. Young JB (2001) Healing the heart with ventricular assist device therapy: mechanisms of cardiac recovery. Ann Thorac Surg 71(3 Suppl):S210–S219. doi:10.1016/S0003-4975(00)02633-3

6. Simon MA, Kormos RL, Murali S, Nair P, Heffernan M, Gorcsan J, Winowich S, McNamara DM (2005) Myocardial recovery using ventricular assist devices: prevalence, clinical characteristics, and outcomes. Circulation 112:I32–I36. doi:10.1161/CIRCULATIONAHA.104.520130

7. Pappas G, Winter SD, Kopriva CJ, Steele PP (1975) Improvement of myocardial and other vital organ functions and metabolism with a simple method of pulsatile flow (IABP) during clinical cardiopulmonary bypass. Surgery 77:34–44

8. Fuchs RM, Brin KP, Brinker JA, Guzman PA, Heuser RR, Yin FC (1983) Augmentation of regional coronary blood flow by intra-aortic balloon counterpulsation in patients with unstable angina. Circulation 68:117–123

9. Gewirtz H, Ohley W, Williams DO, Sun Y, Most AS (1982) Effect of intraaortic balloon counterpulsation on regional myocardial blood flow and oxygen consumption in the presence of coronary artery stenosis: observations in an awake animal model. Am J Cardiol 50:829–837. doi:10.1016/0002-9149(82)91241-3

10. Kern MJ, Aguirre FV, Tatineni S, Penick D, Serota H, Donohue T, Walter K (1993) Enhanced coronary blood flow velocity during intraaortic balloon counterpulsation in critically ill patients. J Am Coll Cardiol 21:359–368

11. Port SC, Patel S, Schmidt DH (1984) Effects of intraaortic balloon counterpulsation on myocardial blood flow in patients with severe coronary artery disease. J Am Coll Cardiol 3:1367–1374

12. Ursulenko VI, Tsyganii AA (1977) Effect of intra-aortic balloon counterpulsation on the hemodynamics and coronary blood flow under conditions of artificial heart rhythm curtailment with the aid of paired electrostimulation. Anesteziol Reanimato 1977:81–84

13. Williams DO, Korr KS, Gewirtz H, Most AS (1982) The effect of intraaortic balloon counterpulsation on regional myocardial blood flow and oxygen consumption in the presence of coronary artery stenosis in patients with unstable angina. Circulation 66:593–597

14. Reesink KD, Sauren LD, Dekker AL, Severdija E, van der Nagel T, Geskes GG, van der Veen FH, Maessen JG (2005) Synchronously counterpulsating extracorporeal life support enhances myocardial working conditions regardless of systemic perfusion pressure. Eur J Cardiothorac Surg 28:790–796. doi:10.1016/j.ejcts.2005.09.006

15. Heldt T, Shim EB, Kamm RD, Mark RG (2002) Computational modeling of cardiovascular response to orthostatic stress. J Appl Physiol 92:1239–1254

16. Schreiner W, Neumann F, Mohl W (1990) The role of intramyocardial pressure during coronary sinus interventions: a computer model study. IEEE Trans Biomed Eng 37:956–967. doi:10.1109/10.102808

17. Hwang CM, Nam KW, Lee JJ, Jeong GS, Ahn CB, Kim KH, Kim BS, Son HS, Fang YF, Sun K (2006) Compact biventricular assist device with pneumatic actuation mechanism. ASAIO J 52:37A

18. Belfus L, Schmitt W, Gruliow R, Rebane T, Folcher MA, Stave S, Gore J (2006) The microcirculation and the lymphatic system: capillary fluid exchange, interstitial fluid, and lymph flow. In: Guyton AC, Hall JE (eds) Textbook of medical physiology. Elsevier, Philadelphia, pp 181–203

19. Schreiner W, Neumann F, Mohl W (1990) Coronary perfusion pressure and inflow resistance have different influence on intramyocardial flows during coronary sinus interventions. Med Phys 17:1023–1031. doi:10.1118/1.596454

20. Monrad ES, Baim DS (1986) Milrinone, dobutamine, and nitroprusside: comparative effects on hemodynamics and myocardial energetic in patients with severe congestive heart failure. Circulation 73(Suppl III):168–172

21. Grosse R, Strain J, Greenberg M (1986) Systemic and coronary effects of intravenous milrinone and dobutaimine in congestive heart failure. J Am Coll Cardiol 7:1107–1113

22. Chidsey CA, Braunwald E (1966) Sympathetic activity and neurotransmitter depletion in congestive heart failure. Pharmacol Rev 18:685–700